Construction and Building Materials 288 (2021) 123082

Contents lists available at ScienceDirect

Construction and Building Materials

journal homepage: www.elsevier.com/locate/conbuildmat

Experimental study and numerical prediction of the bond response of NSM CFRP laminates in RC elements under sustained loading

Javier Gómez *, Cristina Barris, Younes Jahani, Marta Baena, Lluís Torres

AMADE, Polytechnic School, University of Girona, 17003 Girona, Spain

HIGHLIGHTS

- In monotonic pull-out tests, higher strain was observed in specimens with narrower grooves.
- Creep behaviour of adhesive did not depend on the load until 30% of the ultimate load.
- In sustained loading tests, higher slip was obtained as sustained loading increased.
- A time-dependent model was proposed to predict the behaviour of the bonded joint.

ARTICLE INFO

Article history:
Received 8 October 2020
Received in revised form 28 January 2021
Accepted 13 March 2021
Available online 27 March 2021

Keywords:
Near-surface mounted
Fibre-reinforced polymers
Bond behaviour
Sustained loading
Finite differences model

ABSTRACT

This paper presents a study into bond behaviour under sustained loading of Near-Surface Mounted (NSM) Carbon-Fibre Reinforced Polymers (CFRP) concrete joints, through an experimental programme and a numerical analysis. The experimental programme consisted of eight NSM CFRP-concrete pull-out specimens tested under sustained loading and laboratory conditions (20 °C and 55%HR) inside a climatic chamber. Previously, the instantaneous bond behaviour of the NSM CFRP-concrete joint was studied using 18 specimens tested until failure. Furthermore, the tensile behaviour of the adhesive under instantaneous and sustained loading was studied at different loading levels under the same environmental conditions. Finally, a numerical procedure was proposed to predict the bonded joint response under sustained loading. A creep coefficient and a strength reduction factor were applied to the instantaneous bond-slip law to simulate the degrading effect the sustained loading had on the behaviour of the bonded joint. Good agreement between the experimental and numerical results was obtained for the tested parameters, however, further research needs to be carried out in order to extrapolate this methodology to other cases.

1. Introduction

The durability of Reinforced Concrete (RC) structures can be effectively enhanced by employing strengthening techniques such as Externally Bonded Reinforcement (EBR) or Near-Surface Mounted (NSM) reinforcement using Fibre Reinforced Polymer (FRP) strips and bars. Recently, the NSM FRP technique has drawn scientific and industry attention thanks to several advantages it exhibits compared to the EBR FRP technique such as better anchorage capacity and not needing any surface preparation except for grooving [1,2]. Despite this, the main concern when designing NSM FRP strengthened RC structures is to avoid their premature debonding failure.

Although the short-term bond behaviour of the NSM FRP-concrete joint has been widely studied [3–8], less attention has been paid to its long-term performance. However, this is an important area as damaging effects caused by long-term external actions can affect and modify the mechanical performance of the NSM FRP-concrete bonded joint.

In recent years, some authors have experimentally studied the bond behaviour of EBR FRP-concrete joints under sustained loading conditions (Mazzoti *et al.* [9], Ferrier *et al.* [10], Jeong *et al.* [11] and Dash *et al.* [12]). These studies observed that environmental conditions and sustained loading over time had an important effect on the strengthening system's performance. For instance, decreases in the thermomechanical material properties of the bonded joint and strain redistribution along the FRP were observed when elevated temperatures and high sustained loads were applied to EBR FRP-concrete specimens.

* Corresponding author.
E-mail address: javier.gomez@udg.edu (J. Gómez).

https://doi.org/10.1016/j.conbuildmat.2021.123082
0950-0618/

On the other hand, only a few studies into the response of NSM FRP concrete elements under different sustained load levels have been carried out. In one such study, Borchert *et al.* [13] analysed NSM FRP-concrete joints under sustained load and different temperatures and proposed a local bond-slip law for the bonded joint that included a friction branch; adopted from the bond-slip law of deformed reinforcing steel bars [14]. Moreover, they proposed a time-dependent bond-slip law (Fig. 1) where, to consider the long-term effects, the stiffness of the ascending branch, the bond shear strength (τ_{max}) and the residual strength (τ_f) were reduced with time.

Emara *et al.* [15,16], in turn, carried out an experimental study on NSM FRP-concrete elements under sustained loads and different ambient conditions. Their results showed that the combination of high service temperature and high humidity significantly affected the bond behaviour of the joint and so they proposed a damage model for a bilinear bond-slip law, where the stiffness of the ascending branch was reduced with time.

Both models proposed that the softening branch did not vary with time in order to avoid unrealistic increases of fracture energy. Fig. 1 shows the initial bond-slip laws (black curves) and the time-dependent bond-slip laws (red curves) proposed in Borchert *et al.* [13] (Fig. 1a) and Emara *et al.* [15] (Fig. 1b).

It has been widely accepted that the long-term deformations observed in NSM CFRP-concrete joints take place mainly due to the creep performance of the adhesive [15]. Therefore, several studies focussing solely on the creep behaviour of the adhesive under sustained loading and different ambient temperatures can be found in the literature (Costa *et al.* [17–19], Majda *et al.* [20], Meshgin *et al.* [21] and Emara *et al.* [22]). These studies presented the experimental results of tensile tests of resin specimens under sustained loading and concluded that high sustained load levels, together with the ambient conditions and curing times, have an important effect on the thermomechanical properties of the resin. Jeong *et al.* [11,23] and Emara *et al.* [15,22] used the creep coefficient obtained from the long-term adhesive tensile tests to predict the behaviour of FRP-concrete bonded joints under sustained loading. From these studies, higher creep coefficients and strains were observed for specimens under high sustained loading levels and high temperatures and humidity. Moreover, Emara *et al.* [22] observed a linear viscoelastic behaviour of the adhesive up to 60% of the tensile strength under laboratory conditions. On the other hand, Borchert *et al.* [13,24] obtained a creep coefficient from an experimental programme on resin specimens under single shear tests. Results showed a high increase in the resin strain after 1000 h at 20 °C for specimens under 40% of the maximum load.

From this literature review, it can be concluded that even though the long-term behaviour of adhesives under sustained loading has received considerable attention, there is still a lack of knowledge on the overall behaviour of the NSM CFRP-concrete joints under sustained loading and, therefore, more research work needs to be developed in this field.

This paper aims to contribute to the study of the bond behaviour of Carbon-FRP (CFRP) strips bonded to concrete elements under sustained loading. For this purpose, an experimental programme consisting of eight NSM CFRP-concrete elements and nine resin specimens under sustained loading and laboratory conditions (20ºC and 55% RH) has been carried out inside a climatic chamber. A previous experimental programme to evaluate the instantaneous behaviour of the bonded joint and the adhesive behaviour is performed through pull-out and tensile tests, respectively. A numerical methodology has been proposed to analytically predict the bond behaviour of the NSM CFRP-concrete joint under sustained loading. The presented methodology proposes a time-dependent bond-slip law that has been calibrated with the experimental results obtained from the NSM CFRP-concrete and resin tests. Finally, the numerical results obtained from the methodology presented here are shown and conclusions are drawn.

2. Experimental behaviour of the adhesive

In this section, the tensile behaviour of the adhesive used in the NSM CFRP-concrete joint (Sika 30) is characterized through an instantaneous experimental campaign to obtain the corresponding tensile strength and elastic modulus, and a sustained-loading experimental programme designed to study the adhesive's behaviour under service conditions.

2.1. Instantaneous behaviour

To characterize the instantaneous behaviour of the adhesive, six dog-bone resin specimens were cast and cured in accordance with ISO 527-2 [25]. Tensile tests were performed in an MTS Insight 5 kN testing machine at a test speed of 1 mm/min. The instrumentation consisted of one extensometer and two strain gauges placed at both sides of the middle section of the specimen. The test setup and instrumentation are shown in Fig. 2.

The average tensile strength obtained from the instantaneous tests was 27.2 MPa (with a Standard Deviation, SD = 4.5 MPa) and the average maximum strain was 2770 με (SD = 711 με). The average elastic modulus obtained was 10.7 GPa (SD = 471.4 MPa). The average and enveloping stress–strain curves are presented in Fig. 3.

2.2. Sustained loading response

2.2.1. Test setup

To characterize the behaviour of the adhesive under sustained loading, nine dog-bone resin specimens were cast and cured following ISO 527-2 [25]. Three sustained loading levels were

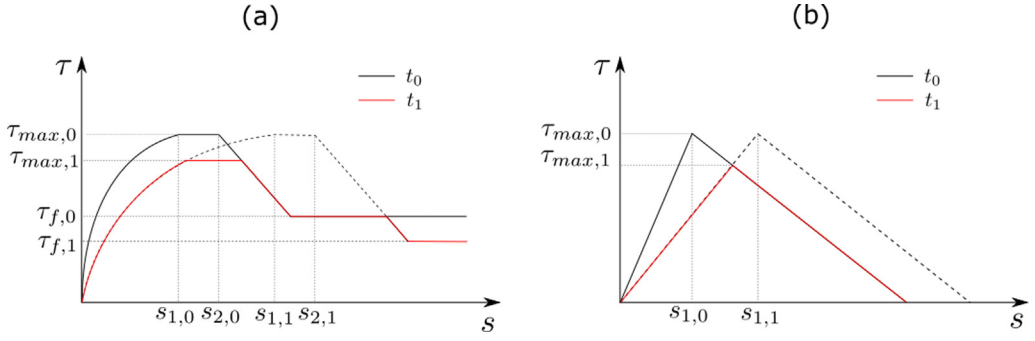

Fig. 1. Time-dependent bond-slip laws proposed in (a) Borchert *et al.* [13] and (b) Emara *et al.* [15].

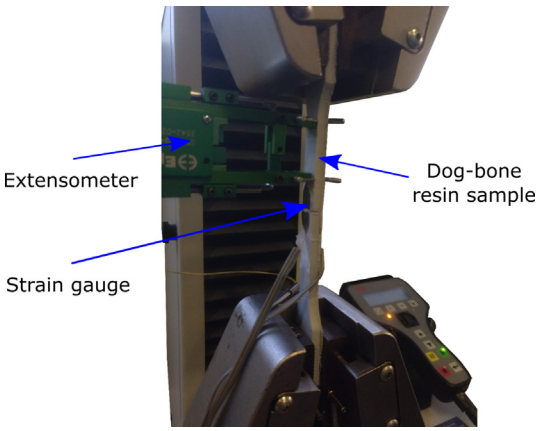

Fig. 2. Test setup and instrumentation of adhesive tensile tests.

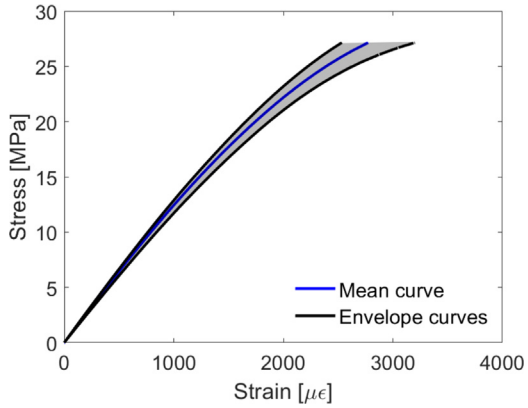

Fig. 3. Stress–strain curve of the instantaneous adhesive tensile test.

applied: 15%, 30% and 50% of the tensile strength previously obtained in the instantaneous tests. Three specimens were tested for each load level. Tests were performed inside a climatic chamber under 55% RH and 20 °C for 1000 h.

The experimental setup for the adhesive sustained-loading test is shown in Fig. 4. The loads were applied using a lever arm with a magnifying factor of 4. Two strain gauges were bonded at each side of the mid-section.

Fig. 4. Experimental test set-up of the adhesive characterization under sustained loading.

2.2.2. Experimental results

Fig. 5 shows the evolution of the axial strain during time for the three levels of sustained loading. Continuous curves represent the average trends from three different samples, while dashed curves correspond to the maximum and minimum enveloping values.

Creep behaviour is defined as a continuous increase of strain under a sustained loading and is usually divided into three stages. The first, also called primary stage, is characterized by a high non-linear increase of strains at a decreasing rate. During the second stage, a linear increase of strain is observed. Finally, the third stage is recognised by an increase of strain at a growing rate until failure [26]. In Fig. 5, two main stages can be identified: the primary stage, where an early high increase of strain can be observed after loading, and the secondary stage, where the increase of strain follows a more linear trend. As expected, as the sustained loading level increases, the strain in the adhesive becomes greater and increases at a higher rate. Furthermore, the final strain results of specimens loaded at 50% of their tensile strength (3124 με) are even higher than the ultimate strain obtained from the instantaneous characterization. This phenomenon was also observed by Costa *et al.* [17], who attributed this effect to the fact that during the sustained-loading tensile tests the resin specimens reorganize their internal structure and thus withstanding the load without failing.

The creep compliance $J_c(t)$, defined as the strain caused by a unit of sustained load, determines whether a viscoelastic material behaves in a linear or non-linear manner with respect to the applied stress. It is calculated as:

$$J_C(t) = \frac{\varepsilon(t)}{\sigma_0} \tag{1}$$

where $\varepsilon(t)$ is the tensile strain during time and σ_0 is the applied stress. The creep compliance for the different sustained loading levels is presented in Fig. 6. Specimens under 15% and 30% of the tensile strength show similar curves, meaning that the strain can be considered proportional to the applied load and that the resin specimens presented a linear viscoelastic behaviour for sustained loading levels up to 30%.

On the other hand, the creep compliance curve for specimens under 50% of the tensile strength is higher than that of the other two load levels. This indicates that the behaviour of specimens under a sustained load of 50% is not in the linear viscoelastic stage.

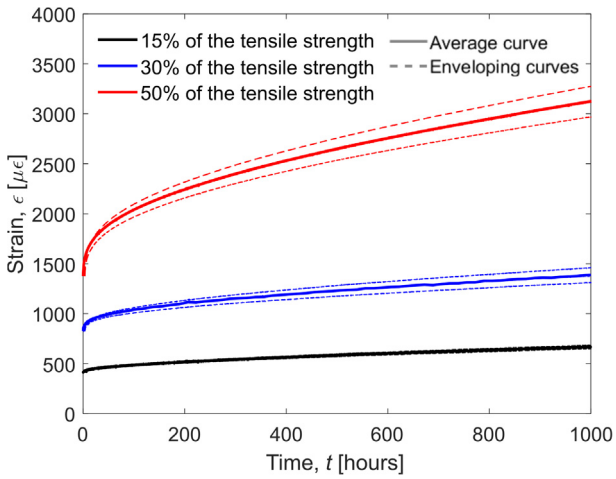

Fig. 5. Evolution of strain in the resin along time.

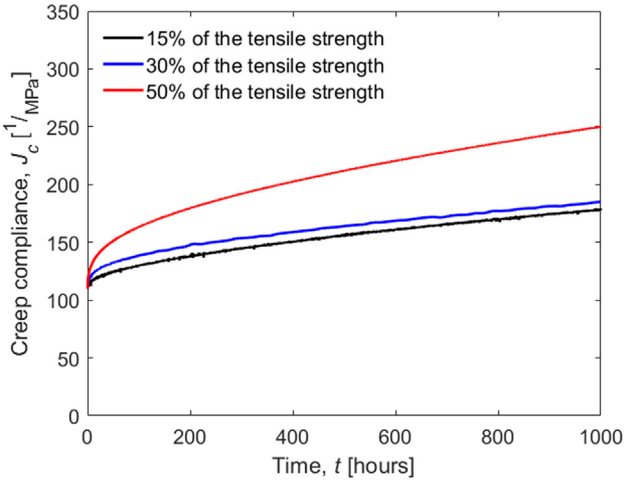

Fig. 6. Experimental creep compliance curves of the adhesive at 15%, 30% and 50% of the tensile strength.

Table 1
Creep coefficient obtained from the sustained loading resin tests.

Time [hours]	1	10	100	1000
Φ(t)	0.04	0.1	0.3	0.7

2.2.3. Adjustment of a creep function

Fig. 6 depicts the increment with time of the strain under sustained loading due to creep.

The creep coefficient was calculated according to Eq. (2) for the different load levels,

$$\Phi(t) = \frac{\varepsilon(t) - \varepsilon(t_0)}{\varepsilon(t_0)} \tag{2}$$

where $\varepsilon(t)$ is the strain along time and $\varepsilon(t_0)$ is the strain at the loading moment. Since the adhesive behaved in a linear viscoelastic stage for a sustained load up to 30% of the tensile strength, the creep coefficient was calculated from the average values obtained from the specimens loaded at 15% and 30% depending on the time. Its values are presented in Table 1. A power function was adjusted to the experimental creep coefficient values, and has been defined as:

$$\Phi(t) = 0.046 \times t^{0.40} \tag{3}$$

where t is the elapsed time in hours. This function was adjusted until t = 1000 h, which was the duration of the test.

3. Bond behaviour of NSM CFRP-concrete joint under sustained loading

This section aims to study the NSM CFRP-concrete bonded joint response under sustained loading. First, the instantaneous behaviour of the bonded joint under a monotonic load until failure is characterised through pull-out tests. The maximum load and failure mode are obtained for each bonded joint configuration.

Next, an experimental study of the bonded joint response for 1000 h at 20 °C and 55% RH is presented. Two different load levels, 15% and 30% of the maximum load, two different groove sizes, 7.5 and 10 mm, and two bonded lengths, 150 and 225 mm, are evaluated.

All specimens were loaded under a single shear pull-out configuration. The increase of slip, defined as the relative displacement between the CFRP laminate and the concrete block, is presented and discussed. The concrete blocks sizes were 200 mm × 200 mm × 370 mm for the short-bonded lengths (L_b = 150 mm) and 200 mm × 200 mm × 420 mm for the long-bonded lengths (L_b = 225 mm and 300 mm).

3.1. Material properties

All specimens were cast from the same concrete batch. Concrete compressive strength and elastic modulus were characterized following ASTM C469 / C469M-10 [27] and UNE 12390–3 [28] standards, obtaining a result of 33.0 MPa (3 specimens, SD = 1.8 MPa) and 33.1 GPa (3 specimens, SD = 1.6 GPa) respectively.

CFRP Sika CarboDur S NSM 1030 strips of 10 mm × 3 mm were used. Six CFRP specimens were characterized according the ISO 527–5 standard [29], obtaining a tensile strength of 3.2 GPa (SD = 68.3 MPa) and an elastic modulus of 169.3 GPa (SD = 13.1 MPa).

The Sika 30 bi-component epoxy resin (previously characterized in Section 2) was used as the adhesive in this experimental campaign.

3.2. Instantaneous bond behaviour of the NSM CFRP-concrete joint

3.2.1. Experimental parameters

To study the short-term behaviour of NSM CFRP-concrete joints, specimens combining two bonded lengths (L_b), 150 mm and 225 mm, and two groove thicknesses (t_g), 7.5 mm and 10 mm, were tested until failure. This section presents an extension of the experimental campaign presented in Gómez *et al.* [30]. Four specimens were tested for each pull-out configuration. To further study the effect of the bonded length, two additional NSM CFRP-concrete specimens with L_b = 300 mm and t_g = 10 mm were also tested. As such, a total of 18 specimens were tested under monotonic loading. Each specimen was labelled ST-L_b-t_g, where ST stands for Short-Term test, L_b for bonded length in mm, and t_g the groove thickness in mm.

The ACI Committee 440 [31] proposes that groove thickness should be equal to or greater than three times the laminate thickness. That said, *fib* Bulletin 90 [32] establishes a minimum groove dimension of 1.5 or 2 times the laminate size to avoid epoxy cover splitting. To study the effect the thickness of the adhesive, two groove widths were used in the experimental programme: 7.5 mm and 10 mm. Taking into account that the laminate thickness is 3.0 mm, the 7.5 mm groove width was set to satisfy the requirement of the *fib*, whilst the 10 mm groove thickness was selected to meet the ACI requirements. Therefore, two adhesive thicknesses were studied: 3.5 mm for the 10 mm grooved specimens, and 2.25 mm for the 7.5 mm grooved specimens. The groove height was set to 15 mm for all cases to comply with the ACI and *fib* requirements of 1.5 times the height of the NSM strip.

Several experimental studies examining the effect of the bonded length and the laminate size [33–36] have been carried out and concluded that the minimum bonded length to achieve the maximum capacity of the bonded joint for laminate sizes similar to those used in this experimental programme ranges between 150 mm and 250 mm. Therefore, the bonded lengths used in the experimental campaign were chosen to be lower and upper bond values of those suggested in the literature.

3.2.2. Test setup

Tests were carried out under a direct pull-out single shear configuration. The short-term setup used in the monotonic tests and a schematic drawing of the setup are shown in Fig. 7a and b, respectively. The top surface of the concrete block was clamped with a 60 mm-wide steel reaction element [37]. To avoid premature

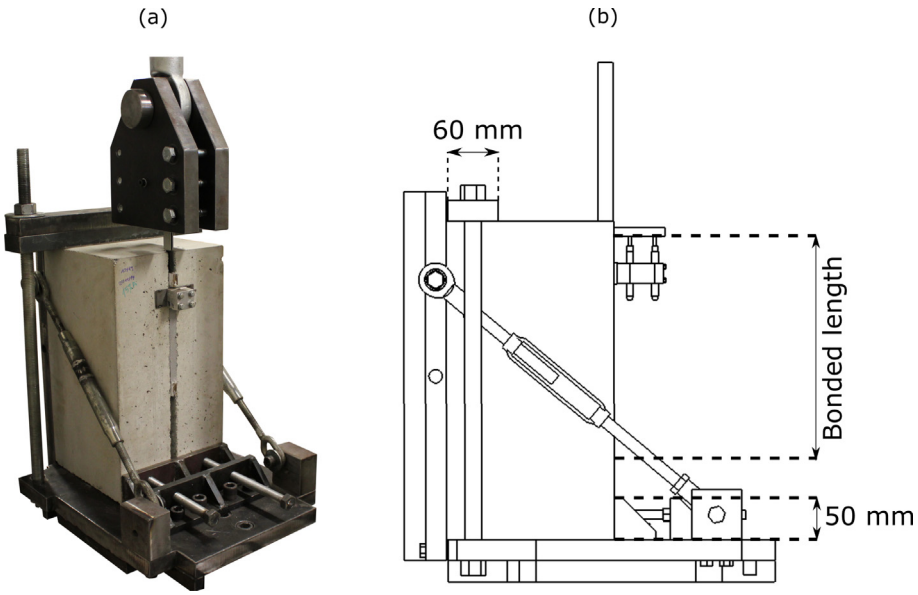

Fig. 7. (a) Set-up of the direct pull-out test and (b) scheme of the set-up.

failure, the concrete blocks were internally reinforced with four 10 mm in diameter steel bars.

3.2.3. Instrumentation

The instrumentation used in the monotonic pull-out tests consisted of one LVDT placed at the loaded end to capture the relative displacement between the CFRP strip and the concrete element.

Additionally, a Digital Image Correlation (DIC) system was installed to register the displacement and strain field of the front surface of the bonded joint during the test. The DIC system has been proven to be an effective tool for measuring displacements and strains in concrete elements [38–40]. A 2D system, consisting of a single camera, was placed perpendicular to the surface of interest to capture the in-plane displacements. Speckle patterns were applied to the samples' front surfaces. Correlation software was used to track all points of the defined surface to obtain the corresponding displacement and strain field. The camera used had a diaphragm aperture of *f*/5.6, and the closing of the diaphragm was 1.000 μsec. The image acquisition frequency used in the test was 1 image/second and the camera's recording resolution was 2452 × 2056 pixels and focal length 23 mm, thus obtaining a conversion factor of 0.114 mm/pixel in the area of interest. A subset of 21 pixels, a step size of 5 pixels, and a Zero-Normalized Cross-Correlation (ZNCC) criteria were used for correlating the images.

3.2.4. Experimental results

The load-slip curves obtained from the short-term tests are shown in Fig. 8, and the average maximum load and failure mode obtained for each NSM CFRP-concrete specimen configuration are presented in Table 2.

It can be observed that for relatively low load levels, while all the specimens followed the same initial trend, differences in the maximum load were obtained. The maximum load increased with the bonded length. It is worth noting that for the 10 mm grooved specimens, the increase in maximum load between specimens with L_b = 150 and 225 mm (ST-150–10 and ST-225–10, respectively) was 27.3%, while the increase between specimens with L_b = 225 and 300 mm (ST-225–10 and ST-300–10, respectively) was 17.7%, indicating that, even though the maximum load increases with the bonded length, this increment is not proportional to the bonded length.

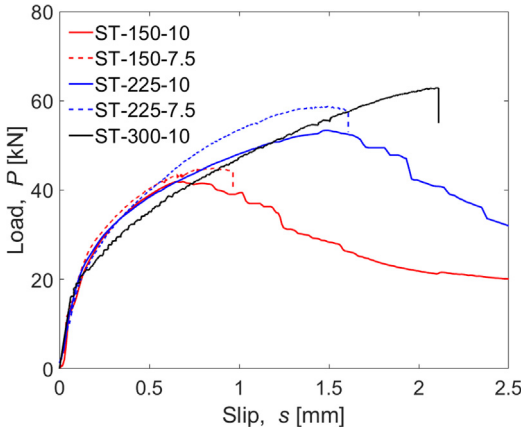

Fig. 8. Experimental average load-slip curves for the short-term pull-out tests.

Table 2
Experimental results of the short-term pull-out tests.

Nomenclature	L_b [mm]	t_g [mm]	Maximum load [kN]	Failure mode
ST-150–10	150	10	41.9	F-A
ST-150–7.5	150	7.5	45.1	C
ST-225–10	225	10	53.3	F-A
ST-225–7.5	225	7.5	58.6	C
ST-300–10	300	10	62.8	F-A

Note: F-A = FRP-adhesive interface, C = cohesive failure in the concrete.

On the other hand, for the same bonded length, specimens with a groove thickness of 10 mm generally achieved a lower maximum load than the 7.5 mm grooved specimens. Additionally, the failure mode was different: 10 mm grooved specimens showed a failure in the FRP-adhesive interface (Fig. 9a), while 7.5 mm grooved specimens presented a cohesive failure in the concrete (Fig. 9b). This behaviour could be attributed to the different shear stiffness (G_a-× t_a, where G_a is the shear modulus of the adhesive and t_a is the adhesive thickness) of the adhesive, which would be higher for the 10 mm grooved specimens and therefore the strain transmitted to the concrete would be lower than in 7.5 mm grooved specimens.

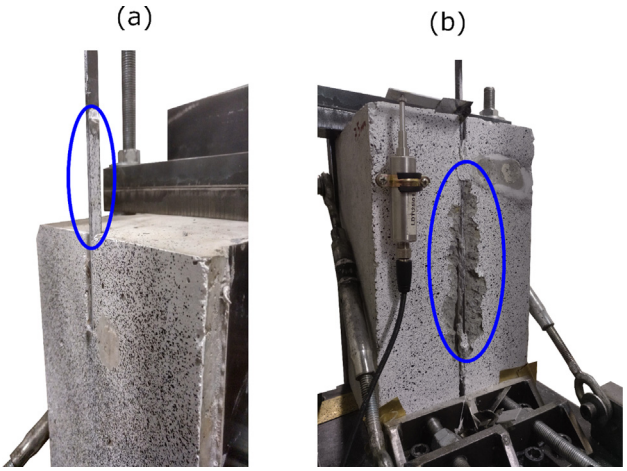

Fig. 9. (a) Failure in the FRP-adhesive interface and (b) cohesive failure in the concrete.

To better understand the differences between the failure modes of the 10 mm and 7.5 mm grooved specimens, Fig. 10a and b present the strain fields in the vertical direction at the maximum load obtained with the DIC 2D system, for an ST-225–10 specimen and an ST-225–7.5 specimen, respectively. In Fig. 10, red lines represent the groove position, and positive values of strain refer to compressive stresses, while negative values indicate tensile stresses.

It can be observed that a maximum strain value of 2000 με and 4500 με was obtained in the concrete surface for the 10 mm and 7.5 mm grooved specimens, respectively. This indicates that, probably, the 7.5 mm grooved specimens achieved their maximum concrete compressive capacity, whilst in the 10 mm grooved samples, the maximum compressive strain of concrete was not achieved.

After the maximum load was achieved, in the 10 mm grooved specimens, because of the residual friction between the FRP and the adhesive, the bonded joint withstood a residual load that smoothly decreased as the slip between the FRP and the concrete increased. This behaviour was not observed in the 7.5 mm grooved specimens, which failed suddenly. Specimens with L_b = 300 mm and t_g = 10 mm also failed by the FRP-adhesive interface, but this time small cracks started to appear in the concrete surrounding the groove, indicating that the compressive stress carried out by the concrete was probably close to the compressive strength.

3.3. Sustained loading response of NSM CFRP-concrete specimens

Eight specimens were tested under a pull-out single shear test configuration, in laboratory conditions and under sustained loading for 1000 h. NSM CFRP-concrete specimens combined two bonded lengths, 150 mm and 225 mm, two groove thicknesses, 7.5 mm and 10 mm and two levels of sustained load, 15% and 30% of the maximum load obtained from the short-term tests.

3.3.1. Test setup and instrumentation

Fig. 11a shows the setup used in the sustained-loading tests while Fig. 11b shows a schematic drawing of the setup. The setup used was an adaptation of the short-term setup, with a lever arm with a multiplying factor of 8.3.

The instrumentation for each specimen consisted of one LVDT placed at the loaded end to capture the slip between the FRP and the concrete and one strain gauge placed at the unbonded loaded end of the laminate to measure the FRP strain either during the loading process or along the testing period.

3.3.2. Experimental parameters

Table 3 summarizes the characteristics and loads for the specimens. Each specimen was labelled LT-L_b-t_g-%P_u, where LT stands for Long-Term and the rest of parameters are the same as those previously defined in Section 3.2.1.

It is worth noting that, even though the load levels applied to the specimens were the same for the 7.5 mm and 10 mm grooved specimens, the maximum load (P_u) for both groove thicknesses was different. Therefore, the load corresponding to 15% or 30% of P_u was different for specimens with different groove thicknesses.

3.3.3. Experimental results

Fig. 12a presents the evolution of slip and Fig. 12b the increase of slip with time for all the NSM CFRP-concrete specimens. Continuous curves represent the 10 mm grooved specimens, and dashed lines the 7.5 mm grooved specimens.

Overall, two main stages in the behaviour of the bonded joints can be identified; a first stage with a high increase of slip with

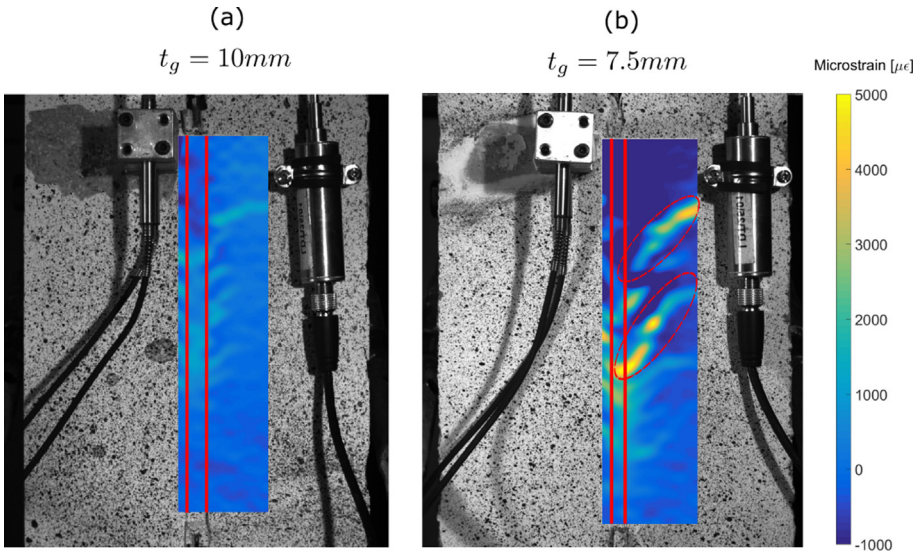

Fig. 10. Strain field in the vertical direction measured by the DIC 2D system for (a) a 10 mm grooved specimen and (b) a 7.5 mm grooved specimen.

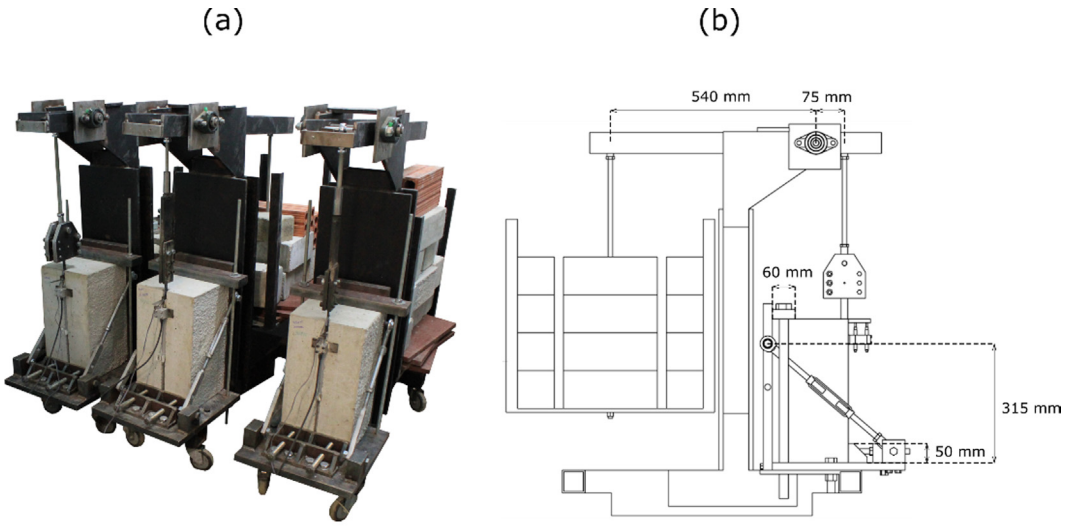

Fig. 11. (a) Image of the set-up for the sustained-loading pull-out test and (b) scheme of the set-up.

Table 3
NSM CFRP-concrete specimens tested under sustained loading.

Nomenclature	L_b [mm]	t_g [mm]	Applied load [kN]	% P_u experimental
LT-150–10-15	150	10	6.4	14.6
LT-150–7.5–15	150	7.5	6.5	13.8
LT-150–10-30	150	10	12.8	29.3
LT-150–7.5–30	150	7.5	14.1	30.0
LT-225–10-15	225	10	8.2	14.9
LT-225–7.5–15	225	7.5	8.9	15.5
LT-225–10-30	225	10	15.2	27.8
LT-225–7.5–30	225	7.5	17.5	30.3

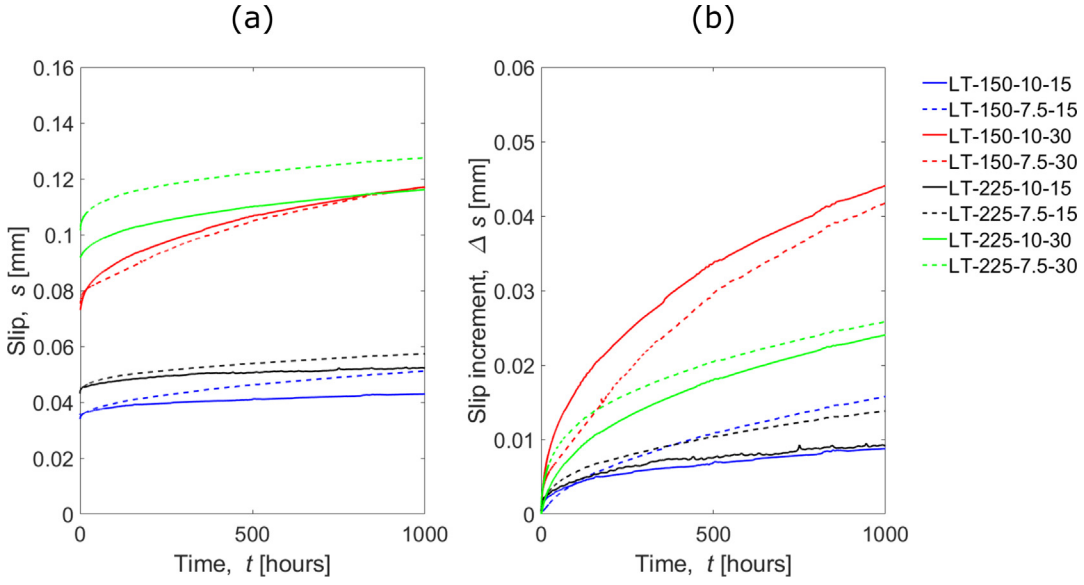

Fig. 12. (a) Total slip at the loaded end and (b) increment of slip with time.

time, and a second stage where the increase of slip becomes more linear [15]. As expected, the specimens loaded at 30% of P_u experimented higher slips than those loaded at 15% of P_u.

Focusing on Fig. 12b, short-bonded length specimens under 30% P_u (red curves) experimented a higher increase of slip with time than their long-bonded length counterparts (green curves) despite being subjected to similar load levels (%P_u). This high increase of slip could be attributed to the fact that the short-bonded length specimens developed a higher average bond shear stress along the FRP, causing more damage to the bonded joint. On the other hand, it can be observed that for a sustained loading level of 15% P_u, the specimens present very similar increases of slip regardless of their bonded length.

Regarding the effect of the groove thickness, similar increases of slip at the loaded end were obtained for specimens with equal bonded lengths and sustained load levels. In general, the 7.5 mm

grooved specimens experienced a higher increase of slip, caused by the fact that they were loaded at higher loads, than their 10 mm counterparts. However, the LT-150–10-30 specimen obtained a higher increment of slip than LT-150–7.5–30, showing a change in the previous tendency for wider adhesive layers in combination with shorter bonded lengths.

4. Numerical methodology to calculate the NSM CFRP-concrete joint response under sustained loading

4.1. Instantaneous bond behaviour of the NSM CFRP-concrete specimens

Based on the short-term bond-slip response, the parameters of idealized typical bilinear bond-slip laws were adjusted using the experimental bond-slip response results [30]. The resulting laws are reproduced in Fig. 13. For the 7.5 mm grooved specimens (with an adhesive layer of 2.25 mm), a bilinear bond-slip law was considered, since a rather sudden failure was obtained once the maximum load was attained. However, for the 10 mm grooved specimens (with an adhesive layer of 3.5 mm), a bilinear bond-slip law including a friction stage was considered to take into account the residual load stage observed during the failure.

As observed in Fig. 13, in comparison with 10 mm grooved specimens, the adjusted bond shear strength (τ_{max}) was higher for specimens with 7.5 mm groove thickness and which is justified by the higher maximum load experimentally obtained.

Fig. 14 presents the theoretical load-slip curves (dashed lines) obtained from a numerical integration procedure, (considering the local bond-slip laws presented in Fig. 13), in comparison with the experimental results (continuous lines) obtained from the pull-out short-term tests. A general good agreement between the numerical and experimental data can be observed.

4.2. Numerical prediction of the bond behaviour under sustained loading

4.2.1. Numerical procedure

The proposed numerical procedure is based on a Finite Differences Model (FDM) and departs from the numerical methodology previously developed for instantaneous bond-slip behaviour.

The methodology divides the bonded length of the FRP-concrete joint into small increments of length, Δx, so as the position, x, of all points at which the equilibrium equations will be assessed is defined. Starting from the loaded end and moving towards the free end, the procedure calculates, for each studied point and for a certain load level, the slip and the load transmitted by Δx taking into account the degradation of the bond-slip law with time (see Section 4.2.2. for further details).

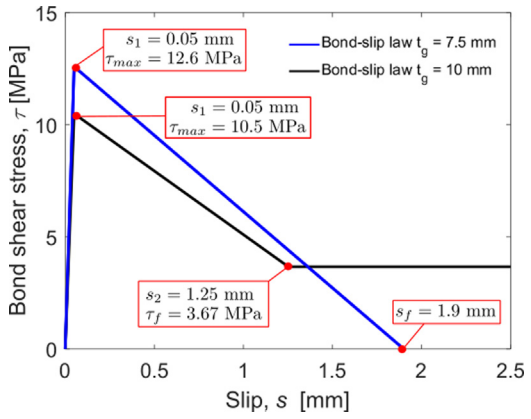

Fig. 13. Bond-slip laws obtained from the experimental monotonic tests.

The differential equation governing the bond–slip behaviour of an NSM FRP-to-concrete bonded joint is [7,41]:

$$\frac{d^2 s(x)}{dx^2} - \frac{\tau(s) \times L_{per}}{E_f \times A_f} = 0 \tag{4}$$

where E_f is the FRP modulus of elasticity, A_f is the FRP cross-section, $\tau(s)$ is the local bond-slip law of the joint and L_{per} is the intermediate perimeter of the adhesive layer [15], calculated using Eq. (5),

$$L_{per} = 2 \times (b_f + t_a) + (t_f + t_a) \tag{5}$$

were b_f is the strip width, t_f is the strip thickness and t_a is the adhesive thickness.

Initially the process defines a load and a slip at the loaded end, which is then used to calculate the strain in the FRP (ε_f), the strain in the concrete (ε_c) and the bond shear stress (τ) using the bond-slip law. The load P at every section along the FRP can be calculated as:

$$P(j,i) = P(j,i-1) - \tau(j,i-1) \times L_{per} \times \Delta x \tag{6}$$

In Eq. (6), the subscript "i" indicates the current point being studied, and the subscript "i-1" refers to the previous studied point, towards the loaded end. Subscript "j" indicates the iteration for a time t. $P(j,1)$ is the sustained load applied to the bonded joint. From the load profile obtained, the strain distribution in the concrete and the FRP can be calculated. Then, the slip profile is calculated as:

$$s(j,i) = s(j,i-1) - (\varepsilon_f - \varepsilon_c) \times \Delta x \tag{7}$$

The convergence condition is that ε_f at the free end must be less than a minimum tolerance, set to be a value close to zero. Otherwise, a new iteration is needed; an increment of slip at the loaded end is added and the process is repeated until the convergence criterion is achieved. Once the equilibrium at time t_i is achieved, the next time step is analysed and the time-dependent bond-slip law is modified. As the numerical procedure is designed for a sustained-load test, the load in the loaded end is kept the same as in the previous step.

The numerical procedure is illustrated in Fig. 15. The red dashed rectangular area indicates the procedure for the instantaneous behaviour, while the steps outside this area refer to the time-dependent degradation of the bond-slip response.

4.2.2. Proposed time-dependent bond-slip law

As observed in the experimental results, the NSM CFRP-concrete joint experiences an increment of slip with time under sustained loading. In this work, this effect is attributed to a reduction in time-dependent effective stiffness ($K_e(t)$) and bond shear strength ($\tau_{max}(t)$), which are defined similarly as in [13,15]. To avoid an unrealistic increase of fracture energy, the softening branch of the proposed time-dependent bond-slip law is maintained as the softening branch at t_0 [42]. Fig. 16 shows the approximate shapes for the resultant time-dependent bilinear (Fig. 16a) and bilinear plus friction (Fig. 16b) bond-slip laws, where $s_{1,0}$ is the initial slip at the bond shear strength τ_{max}, and $s_{1,1}$ is the slip at the bond shear stress at t_1. Black and red curves represent the bond-slip laws at t_0 and t_1, respectively.

The proposed model is governed by two parameters: a creep coefficient $\Phi(t)$ that reduces the effective stiffness, and a strength reduction coefficient ($f(t)$) that reduces the bond shear strength.

The reduction of the stiffness of the ascending branch of the bond-slip law is carried out by using the Effective Modulus Method (EMM), as follows:

$$K_e(t) = \frac{K_{e,0}}{(1 + \Phi(t))} \tag{8}$$

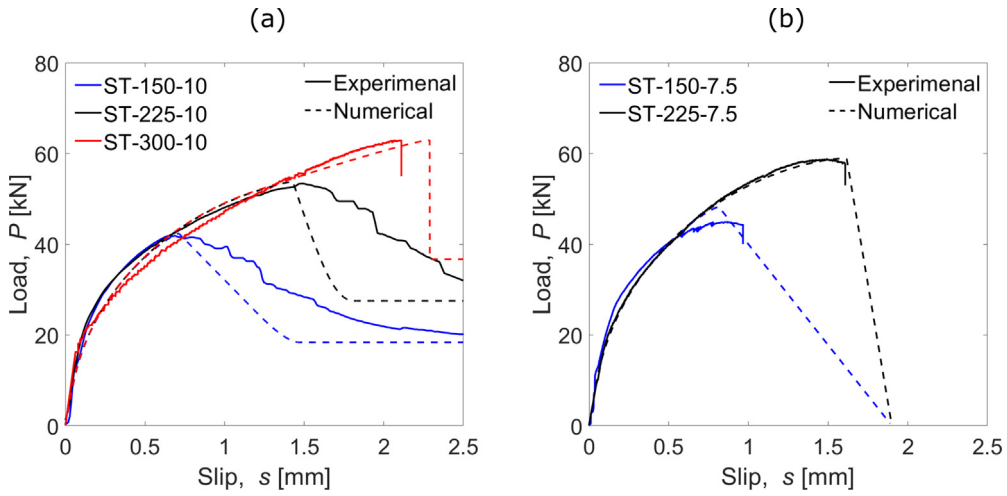

Fig. 14. Comparison of experimental and numerical results for (a) 10 mm grooved specimens and (b) 7.5 mm grooved specimens.

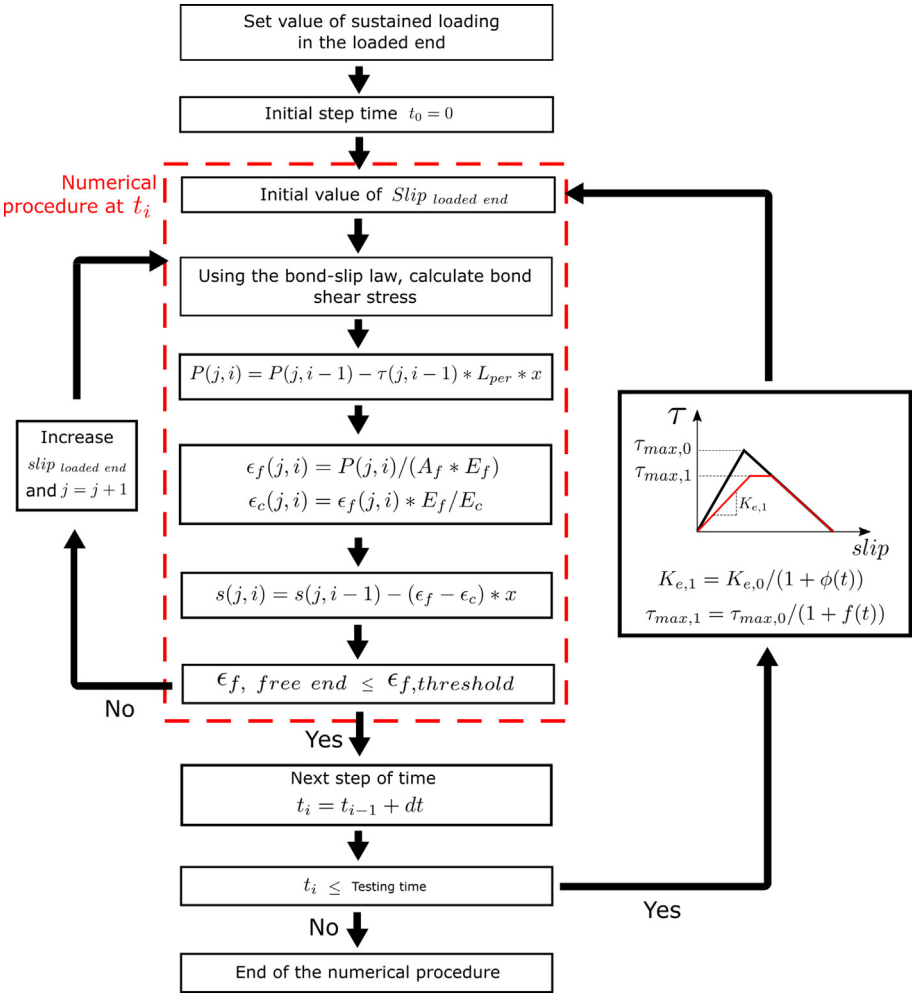

Fig. 15. Flowchart of the numerical procedure.

where $K_e(t)$ is the time-dependent stiffness at time t and $K_{e,0}$ is the initial stiffness. As the stiffness of the bond-slip law is mainly dependent on the adhesive creep behaviour, the creep coefficient $\Phi(t)$ has been determined from the resin tests under sustained loading.

On the other hand, the bond shear strength $\tau_{max}(t)$ is reduced with time as:

$$\tau_{max}(t) = \tau_{max,0} \times a(t) \tag{9}$$

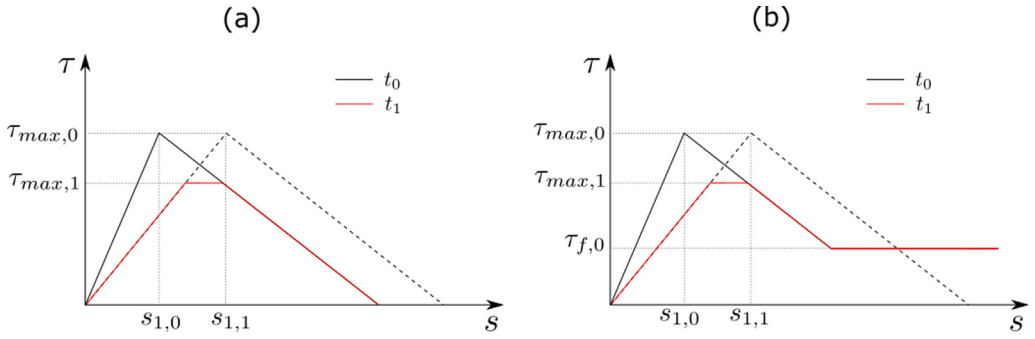

Fig. 16. Time-dependent bond-slip models: (a) a bilinear model and (b) a bilinear plus friction model.

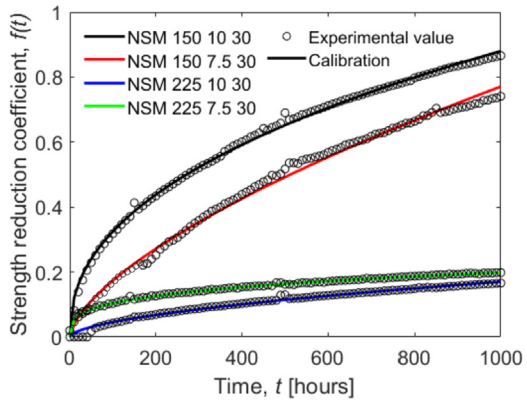

Fig. 17. Strength reduction coefficient evolution with time for each specimen.

where $\tau_{max,0}$ is the initial bond strength at loading, and $a(t)$ is defined as:

$$a(t) = \frac{1}{1+f(t)} \tag{10}$$

with $f(t)$ being a strength reduction coefficient. The coefficient $f(t)$ is obtained from the experimental results and it is shown in Fig. 17 for specimens under 30% of P_u. The shape of these curves can be described by a power function as follows:

$$f(t) = \alpha \times t^{\beta} \tag{11}$$

where t is the elapsed time in the sustained loading test in hours, α is a scaling factor and β is a parameter that controls the rate of growth of the function.

4.2.3. Calibration of the strength reduction factor parameters α and β

The calibration of parameters α and β has been performed by means of the least-square differences method and the obtained $f(t)$ coefficient is shown in Fig. 17 in continuous lines. The resultant time-dependent bond-slip law is presented in Fig. 18 for specimens LT-150–7.5 loaded at 30% (Fig. 18a) and 15% (Fig. 18b) at different time steps (0, 250, 500, 750 and 1000 h). A red dot indicates the stress-slip situation of the loaded end. For specimens under 30% of P_u, the loaded end has already surpassed the point of τ_{max} at t = 0 h (Fig. 18a). However, for specimens loaded at 15% of P_u, the strength reduction does not affect the overall time-dependent behaviour because the loaded end did not reach the maximum bond shear strength τ_{max}, as is observed in Fig. 18b. This effect was noticed in all specimens loaded at 15% P_u. Since the values obtained for β ranged between 0.35 and 0.55, for the sake of simplicity an average value of 0.45 is adopted. With this simplification, a comparison between the numerical and experimental values of the slip at the loaded end is shown in Fig. 19. Continuous and dashed lines represent the experimental and numerical values, respectively. A general good agreement can be observed between the experimental data and the numerical predictions.

4.2.4. Application of the numerical methodology to other experimental studies

In this section, the proposed methodology is extended to predicting the experimental results presented in [15], which was

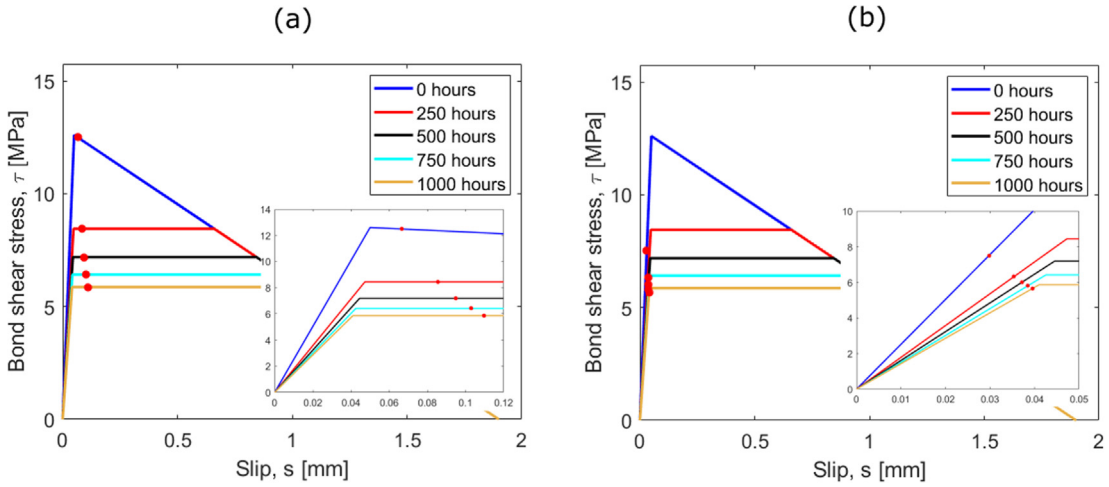

Fig. 18. Evolution of the local bond-slip law with time for (a) LT-150–7.5–30 and (b) LT-150–7.5–15 specimens.

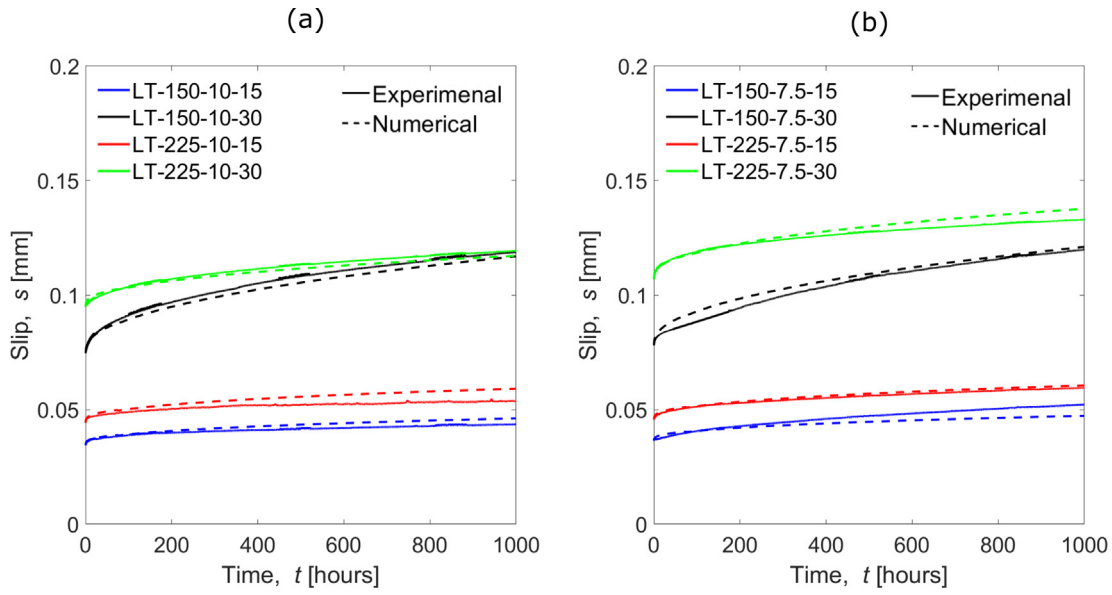

Fig. 19. Comparison of the experimental and numerical slip at the loaded end (a) for 10 mm grooved specimens and (b) for 7.5 mm grooved specimens obtained in the present study.

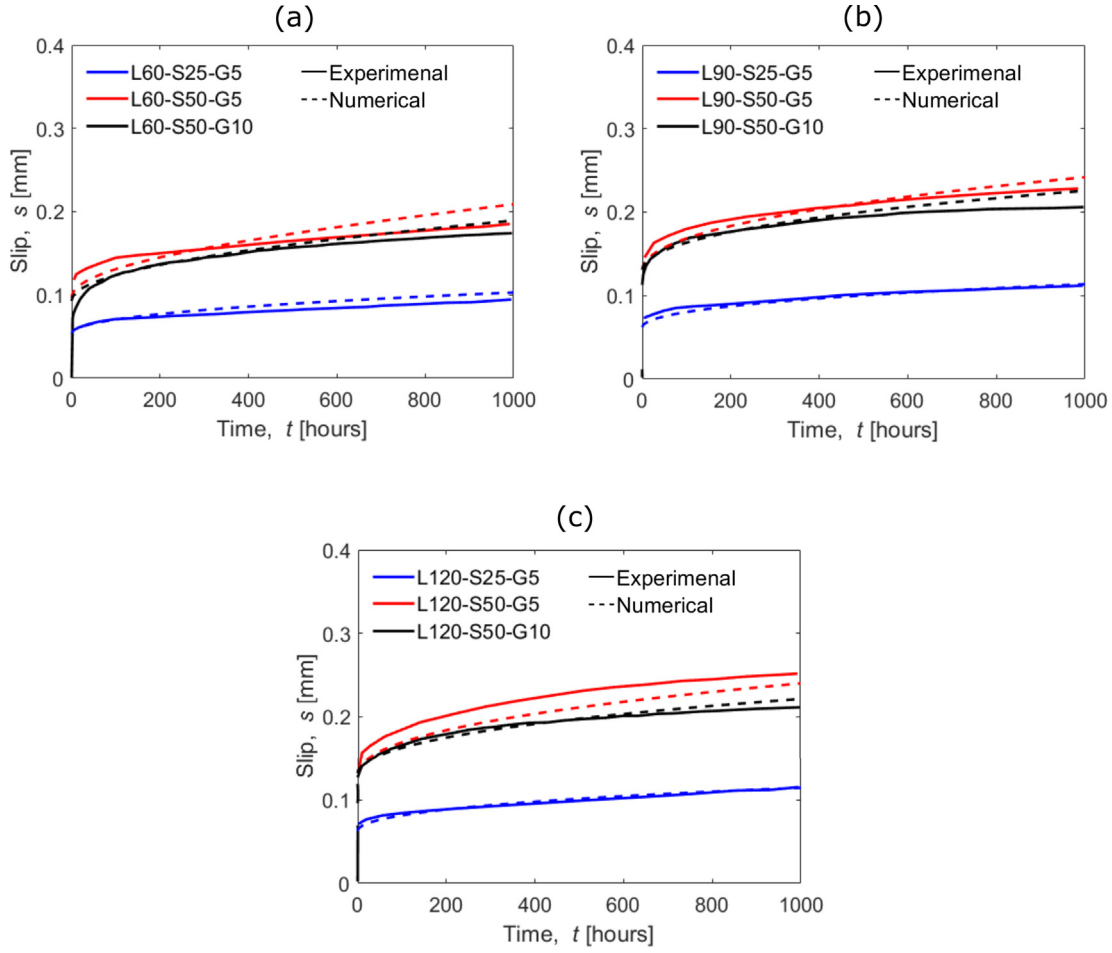

Fig. 20. Comparison between the numerical and experimental values for specimens with (a) L_b = 60 mm, (b) L_b = 90 mm and (c) L_b = 120 mm obtained in [15].

focused on the effect groove thickness, bonded length and sustained loading level have on the behaviour of NSM CFRP concrete specimens under sustained loading and room conditions. In that study, a different epoxy adhesive type (E_f = 6600 MPa, f_{fu} = 20 MPa), CFRP material (E_f = 160 GPa, f_{fu} = 2400 MPa) with a different section (10 mm × 1.4 mm), groove thicknesses (5 mm and 10 mm), bonded lengths (60 mm, 90 mm and 120 mm) and sustained load levels (25% and 50% of P_u), were used. Specimens were labelled

L-S-G, where L stands for the bonded length, S the sustained load level and G the groove thickness.

Values of the parameter α are obtained (as indicated in the previous section) considering β = 0.45, and the resultant theoretical evolution of slip with time is shown in Fig. 20, together with the experimental values.

Since the strength reduction coefficient is dependent on the applied load, the average bond shear stress (τ_{avg}) is taken as a reference variable:

$$\tau_{avg} = \frac{P}{L_b \times L_{per}} \quad (12)$$

and compared to the previously obtained parameter α (Table 4). As expected, a general increasing trend of α with the increase of τ_{avg} is observed, although two ranges of τ_{avg} can be identified, each one for the two different experimental campaigns.

In order to propose a model suitable to be extrapolated to other results, a non-dimensional parameter τ_{avg}/τ_{max} is defined. In Fig. 21, the relationship between α and τ_{avg}/τ_{max} is shown. Regardless of the scatter of the data, an ascending tendency can be observed, meaning that as the average shear stress in the bonded joint increases α, and consequently the strength reduction coefficient, increase as well, causing a higher reduction on the time-dependent bond strength. Even though a relationship between α and τ_{avg}/τ_{max} has been observed in this study, as it was based on a limited number of specimens, more experimental tests should be carried out to further assess this relationship. Finally, it should be mentioned that due to the nature of the single shear pull-out configuration test, the possible effect of cracking is not directly included in the tests. Cracking in beams is a phenomenon taking place at relatively low loads and crack spacing tends to decrease as the load increases. For considering cracking effect, new series of tests with different bonded lengths should be carried out to compare the influence on the response.

Table 4
Values of α and τ_{avg} obtained considering β = 0.45.

Specimen	$\alpha \times 100$	τ_{avg} [MPa]
LT-L150-t10-P30	3.9	2.7
LT-L150-t7.5-P30	3.2	3.2
LT-L225-t10-P30	0.7	2.3
LT-L225-t7.5-P30	0.9	2.5
L60-S50-G5	6.0	6.5
L60-S50-G10	5.5	6.0
L90-S50-G5	4.0	5.4
L90-S50-G10	3.0	5.0
L120-S50-G5	4.0	4.1
L120-S50-G10	2.5	3.7

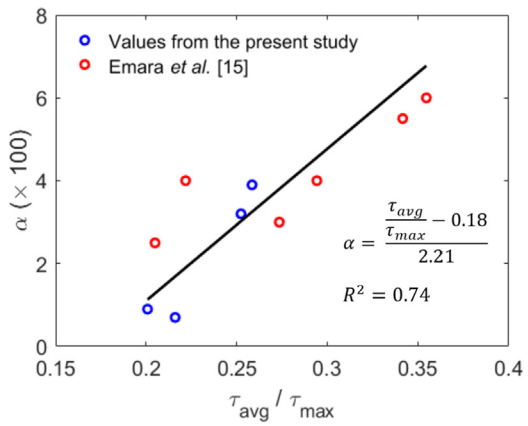

Fig. 21. Relationship between α - τ_{avg}/τ_{max}.

5. Conclusions

This work aimed to study the behaviour of NSM CFRP-concrete bonded joints under sustained loading and laboratory conditions. Pull-out and dog-bone adhesive specimens were subjected to sustained loading for 1000 h. A numerical procedure based on FDM to predict the bond behaviour under sustained loading based on a time-dependent local bond-slip was proposed and validated. Based on the analysis of the experimental results and corresponding range of parameters presented in this work the following conclusions are drawn.

From the adhesive specimens tested under tensile sustained loading, it can be concluded that:

- Adhesive specimens loaded up to 30% of P_u were under a linear creep stage, meaning that the creep behaviour did not depend on the applied load.
- A creep coefficient was adjusted with a power function from specimens loaded at 15% and 30% of P_u.

From the sustained loading tests of the NSM CFRP-concrete specimens, the following conclusions can be drawn:

- As expected, specimens under 30% of P_u experimented a higher increase of slip in comparison to specimens under 15% of P_u.
- Short-bonded length specimens under 30% of P_u experimented a higher increase of slip than long-bonded length specimens. However, no effect of the bonded length was observed in specimens under 15% of P_u.

From the proposed numerical procedure with which to model the NSM CFRP-concrete joint bond response under sustained loading, it can be concluded that:

- A time-dependent bond slip law based on a strength reduction factor and a creep coefficient is proposed to predict the behaviour of the bonded joint.
- The strength reduction factor was adjusted through a power function defined by two parameters: α and β. While parameter β could be experimentally adjusted to a mean value of 0.45, an increasing relationship between the average bond stress normalized with the bond shear strength, τ_{avg}/τ_{max}, and parameter α was able to be identified.
- Specimens under 15% of P_u were not affected by the strength reduction factor. In these cases, the time-dependent behaviour was only governed by the creep coefficient.
- Further experimental tests at service loading levels are needed to better explore the relationship between τ_{avg}/τ_{max} and α.

The experimental series carried out and the corresponding selected range of parameters allowed the conclusions above to be reached. However, further research is needed to expand the number of tests and parameters.

CRediT authorship contribution statement

Javier Gómez: Conceptualization, Formal analysis, Data curation, Investigation, Methodology, Writing - original draft. **Cristina Barris:** Conceptualization, Methodology, Supervision. **Younes Jahani:** Validation, Investigation. **Marta Baena:** Investigation, Validation. **Lluís Torres:** Supervision.

Declaration of Competing Interest

The authors declare that they have no known competing financial interests or personal relationships that could have appeared to influence the work reported in this paper.

Acknowledgements

This work was supported by the Spanish Government (MINECO) [Project Ref. BIA2017-84975-C2-2-P]; the University of Girona [grant number IFUdG2018/28]; and the Generalitat de Catalunya [grant number 2019FI_B 00054]. The authors also wish to acknowledge the support of SIKA for supplying the strips and the epoxy adhesive used in this study.

References

[1] L. De Lorenzis, J.G. Teng, Near-surface mounted FRP reinforcement: an emerging technique for strengthening structures, Compos. Part B Eng. 38 (2007) 119–143, https://doi.org/10.1016/j.compositesb:2006.08.003.
[2] G.M. Dalfré, J.A.O. Barros, NSM technique to increase the load carrying capacity of continuous RC slabs, Eng. Struct. 56 (2013) 137–153, https://doi.org/10.1016/j.engstruct.2013.04.021.
[3] L. De Lorenzis, A. Rizzo, A. La Tegola, A modified pull-out test for bond of near-surface mounted FRP rods in concrete, Compos. Part B Eng. 33 (2002) 589–603, https://doi.org/10.1016/S1359-8368(02)00052-5.
[4] J.M. Sena Cruz, J.A.O. Barros, R. Gettu, Á.F.M. Azevedo, Bond behavior of near-surface mounted CFRP laminate strips under monotonic and cyclic loading, J. Compos. Constr. 10 (2006) 295–303, https://doi.org/10.1061/(ASCE)1090-0268(2006)10:4(295).
[5] A. Bilotta, F. Ceroni, J.A.O. Barros, I. Costa, A. Palmieri, Z.K. Szabó, E. Nigro, S. Matthys, G.L. Balazs, M. Pecce, Bond of NSM FRP-strengthened concrete: round robin test initiative, J. Compos. Constr. 20 (2016) 04015026, https://doi.org/10.1061/(ASCE)CC.1943-5614.0000579.
[6] F. Ceroni, M. Pecce, A. Bilotta, E. Nigro, Bond behavior of FRP NSM systems in concrete elements, Compos. Part B Eng. 43 (2012) 99–109, https://doi.org/10.1016/j.compositesb:2011.10.017.
[7] M.S. Mohamed Ali, D.J. Oehlers, M.C. Griffith, R. Seracino, Interfacial stress transfer of near surface-mounted FRP-to-concrete joints, Eng. Struct. 30 (2008) 1861–1868, https://doi.org/10.1016/j.engstruct.2007.12.006.
[8] D. Novidis, S.J. Pantazopoulou, E. Tentolouris, Experimental study of bond of NSM-FRP reinforcement, Constr. Build. Mater. 21 (2007) 1760–1770, https://doi.org/10.1016/j.conbuildmat.2006.05.054.
[9] C. Mazzotti, M. Savoia, Long term properties of bond between concrete and Frp, Concrete 1–3 (2005) 531–538.
[10] E. Ferrier, L. Michel, B. Jurkiewiez, P. Hamelin, Creep behavior of adhesives used for external FRP strengthening of RC structures, Constr. Build. Mater. 25 (2011) 461–467, https://doi.org/10.1016/j.conbuildmat.2010.01.002.
[11] Y. Jeong, J. Lee, W.S. Kim, Modeling and measurement of sustained loading and temperature-dependent deformation of carbon fiber-reinforced polymer bonded to concrete, Materials (Basel) 8 (2015) 435–450, https://doi.org/10.3390/ma8020435.
[12] S. Dash, Y. Jeong, M.M. Lopez, C.E. Bakis, Experimental Characterization of Moisture , Temperature and Sustained Loading on Concrete-FRP Bond Performance, in: J. Barros, J.M. Sena-Cruz (Eds.), Proc. 11th Int. Symp. Fiber Reinf. Polym. Reinf. Concr. Struct. - FRPRCS-11, Guimarães (Portugal), 2013: pp. 1–7.
[13] K. Borchert, K. Zilch, Bond behaviour of NSM FRP strips in service, Struct. Concr. 9 (2008) 127–142, https://doi.org/10.1680/stco.2007.00015.
[14] R. Eligehausen, E.P. Popov, V.V. Bertero, Local bond stress-slip relationships of deformed bars under generalized excitations, Earthq. Eng. Res. Cent. 4 (1982) 69–80.
[15] M. Emara, C. Barris, M. Baena, L. Torres, J. Barros, Bond behavior of NSM CFRP laminates in concrete under sustained loading, Constr. Build. Mater. 177 (2018) 237–246, https://doi.org/10.1016/j.conbuildmat.2018.05.050.
[16] M. Emara, L. Torres, M. Baena, C. Barris, X. Cahís, Bond response of NSM CFRP strips in concrete under sustained loading and different temperature and humidity conditions, Compos. Struct. 192 (2018) 1–7, https://doi.org/10.1016/j.compstruct.2018.02.048.
[17] I. Costa, J. Barros, Tensile creep of a structural epoxy adhesive: experimental and analytical characterization, Int. J. Adhes. Adhes. 59 (2015) 115–124, https://doi.org/10.1016/j.ijadhadh.2015.02.006.
[18] I. Costa, J. Barros, Creep of structural adhesives: an overview, in: Proc. 6th Int. Conf. FRP Compos. Civ. Eng. CICE 2012, 2012: pp. 1–8. http://repositorium.sdum.uminho.pt/handle/1822/21567.
[19] I.G. Costa, J.A.O. Barros, Assessment of the long term behaviour of structural adhesives in the context of NSM flexural strengthening technique with prestressed CFRP laminates, in: J.B.& J. Sena-Cruz (Ed.), Proc. 11th Int. Symp. Fiber Reinf. Polym. Reinf. Concr. Struct. - FRPRCS-11, Guimarães, 2013: pp. 1–10.
[20] P. Majda, J. Skrodzewicz, A modified creep model of epoxy adhesive at ambient temperature, Int. J. Adhes. Adhes. 29 (2009) 396–404, https://doi.org/10.1016/j.ijadhadh.2008.07.010.
[21] P. Meshgin, K.-K. Choi, M.M. Reda Taha, Experimental and analytical investigations of creep of epoxy adhesive at the concrete-FRP interfaces, Int. J. Adhes. Adhes. 29 (2009) 56–66, https://doi.org/10.1016/j.ijadhadh.2008.01.003.
[22] M. Emara, L. Torres, M. Baena, C. Barris, M. Moawad, Effect of sustained loading and environmental conditions on the creep behavior of an epoxy adhesive for concrete structures strengthened with CFRP laminates, Compos. Part B Eng. 129 (2017) 88–96, https://doi.org/10.1016/j.compositesb.2017.07.026.
[23] Y. Jeong, M.M. Lopez, C.E. Bakis, Effects of temperature and sustained loading on the mechanical response of CFRP bonded to concrete, Constr. Build. Mater. 124 (2016) 442–452, https://doi.org/10.1016/j.conbuildmat.2016.07.123.
[24] K. Borchert, K. Zilch, Time depending thermo mechanical bond behavior of epoxy bonded pre-stressed FRP-reinforcement, Proc. 7th Int. Symp. Fiber Reinf. Polym. Reinf. Concr. Struct. (2005) FRPRCS671–7683.
[25] ISO 527-2:2012, Determination of tensile properties-Part 2: Test conditions for moulding and extrusion plastics, Geneva, Switzerland, 2012.
[26] W.N. Findley, J.S. Lai, K. Onaran, R.M. Christensen, Creep and Relaxation of Nonlinear Viscoelastic Materials With an Introduction to Linear Viscoelasticity, Dover Publications, New York, 1979. DOI:10.1115/1.3424077.
[27] ASTM C469 / C469M-10, Standard Test Method for Static Modulus of Elasticity and Poisson's Ratio of Concrete in Compression, West Conshohocken, PA, 2010.
[28] UNE 12390-3, Testing hardened concrete. Part 3: Compressive strength of test specimens., AENOR, Madrid, 2003.
[29] ISO 527-5:2009, Determination of tensile properties - Part 5: Test conditions for unidirectional fibre-reinforced plastic composites, Geneva, Switzerland, 2009.
[30] J. Gómez, L. Torres, C. Barris, Characterization and simulation of the bond response of NSM FRP reinforcement in concrete, Materials (Basel) 13 (7) (2020) 1770, https://doi.org/10.3390/ma13071770.
[31] ACI 440.2R-08, Guide for the design and construction of externally bonded FRP systems for strengthening existing structures, American Concrete Institute, 2008.
[32] fib bulletin 90, Externally applied FRP reinforcement for concrete structures, International Federation for Structural Concrete, 2019.
[33] F. Ceroni, J.A.O. Barros, M. Pecce, M. Ianniciello, Assessment of nonlinear bond laws for near-surface-mounted systems in concrete elements, Compos. Part B Eng. 45 (1) (2013) 666–681, https://doi.org/10.1016/j.compositesb:2012.07.006.
[34] A. Bilotta, F. Ceroni, M. Di Ludovico, E. Nigro, M. Pecce, G. Manfredi, Bond efficiency of EBR and NSM FRP systems for strengthening concrete members, J. Compos. Constr. 15 (2011) 757–772, https://doi.org/10.1061/(ASCE)CC.1943-5614.0000204.
[35] R. Seracino, N.M. Jones, M.S. Ali, M.W. Page, D.J. Oehlers, Bond strength of near-surface mounted FRP strip-to-concrete joints, J. Compos. Constr. 11 (4) (2007) 401–409, https://doi.org/10.1061/(ASCE)1090-0268(2007)11:4(401).
[36] S.S. Zhang, J.G. Teng, T. Yu, Bond strength model for CFRP strips near-surface mounted to concrete, J. Compos. Constr. 18 (2014), https://doi.org/10.1061/(ASCE)CC.1943-5614.0000402.
[37] C. Mazzotti, M. Savoia, B. Ferracuti, A new single-shear set-up for stable debonding of FRP-concrete joints, Constr. Build. Mater. 23 (4) (2009) 1529–1537, https://doi.org/10.1016/j.conbuildmat.2008.04.003.
[38] M. Di Bendetti, J. Gómez, S. Cholostiakow, H. Fergani, C. Barris, M. Guadagnini, Reliability of DIC measurements for the structural monitoring of FRP RC elements, in: 9th Int. Conf. Fibre-Reinforced Polym. Civ. Eng. (CICE 2018), PARIS 17-19 JULY 2018, 2018.
[39] M. Di Benedetti, M. Guadagnini, J. Gómez, C. Barris, L. Torres, Experimental study on the DIC setup for the analysis of FRP RC members, in: Adv. Compos. Constr. ACIC 2017 - Proc. 8th Bienn. Conf. Adv. Compos. Constr., 2017.
[40] C. Barris, L. Torres, I. Vilanova, C. Miàs, M. Llorens, Experimental study on crack width and crack spacing for Glass-FRP reinforced concrete beams, Eng. Struct. 131 (2017) 231–242, https://doi.org/10.1016/j.engstruct.2016.11.007.
[41] H. Yuan, J.G. Teng, R. Seracino, Z.S. Wu, J. Yao, Full-range behavior of FRP-to-concrete bonded joints, Eng. Struct. 26 (5) (2004) 553–565, https://doi.org/10.1016/j.engstruct.2003.11.006.
[42] Comité Euro-International du Betón, CEB-1997. Serviceability Models - Behaviour and modelling in serviceability limit states including repeated and sustained load sustained loads. CEB, Bulletin d'information No. 235, Lausanne, Switzerland, 1997.